

## **UNIT IV PERMANENT MAGNET MOTORS**

### **4.1 INTRODUCTION**

The use of permanent magnets in construction of electrical machines brings the following benefits

- No electrical energy is absorbed by the field excitation system and thus there is no excitation loss which means substantial increase in the efficiency.
- Higher torque and/or output power per volume than when using electromagnetic excitation.
- Better dynamic performance than motors with electromagnetic excitation.
- Simplification of construction and maintenance
- Reduction of prices for some types of machines

### **4.2 PERMANENT MAGNET MATERIALS**

There are three classes of permanent magnets currently used for electric motors

- Alnicos (Al, Ni, Co, Fe);
- Ceramics (Ferrites) e.g. Barium ferrite  $BaO \times 6Fe_2O_3$  and Strontium ferrite  $SrO \times 6Fe_2O_3$ .
- Rare earth materials i.e. Samarium cobalt SmCo and neodymium iron boron NdFeB.

### **4.3 TYPES OF PERMANENT MAGNET MOTORS DRIVES**

There are three types of permanent magnet motor electromechanical drives they are

- DC Commutator motor drives.
- Brushless motor drives.
  - ✓ Square Wave Permanent magnet brushless motor drives (also called as PMBLDC).
  - ✓ Sine Wave Permanent magnet brushless motor drives (also called as PMSM).
- Stepping motor drives.

### **4.4 APPLICATION OF PERMANENT MAGNET MOTORS**

Permanent magnet motors are used in broad range from mW's to hundreds of KW's. There are also attempts to apply PMs to large motors rated at minimum 1 MW. The application of PM electric motor includes.

- ✓ Industrial drives (e.g.) Pumps, Fans, blowers, compressors etc
- ✓ Air-conditioning systems, Auto bank machines, Ticketing machines, Bar-code readers at supermarkets etc.
- ✓ Washing machines and cloth dryers, Vacuum cleaners, toys etc.

## 4.5 SQUARE WAVE PM BRUSHLESS MOTOR DRIVES (BLDC MOTORS)

### 4.5.1 Why brushless D.C.?

The brushless D.C. motor is shown in its most usual form in Figure 4.1 alongside the PM D.C. commutator motor. The stator structure is similar to that of a polyphase a.c. induction motor. The function of the magnet is the same in both the brushless motor and the D.C. commutator motor. In both cases the air gap flux is ideally fixed by the magnet and little affected by armature current.

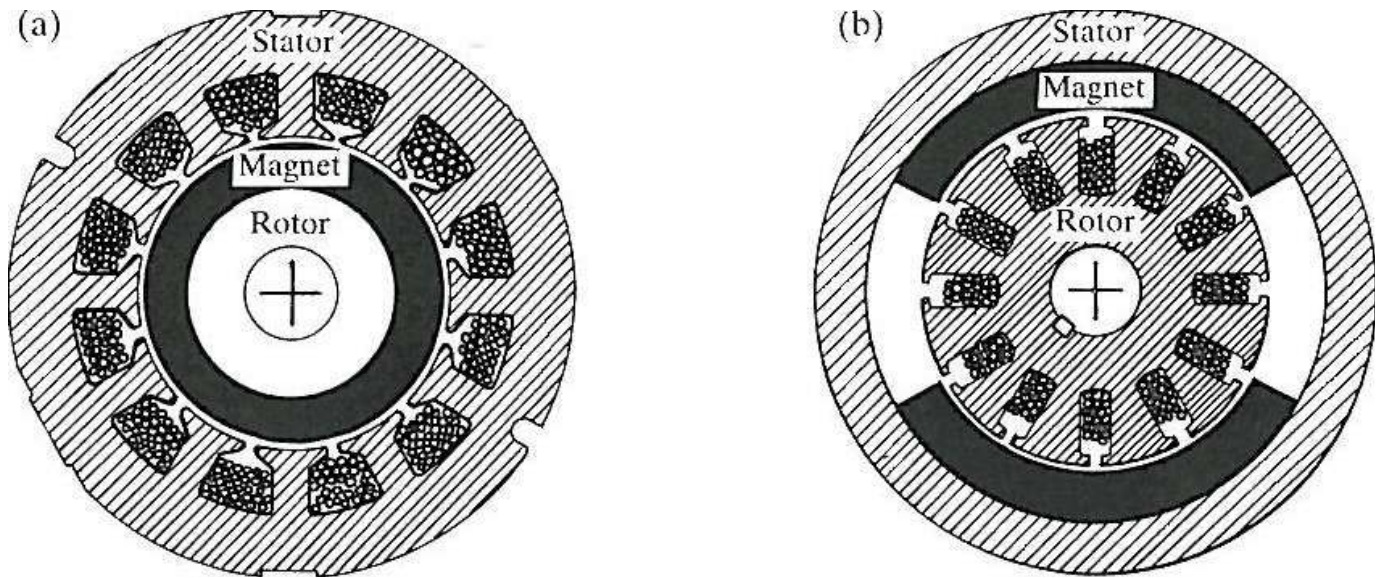


FIG. 4.1. (a) Brushless D.C. motor and (b) PM D.C. commutator motor.

The most obvious advantage of the brushless configuration is the **removal of the brushes**. Brush **maintenance is no longer required**, and many problems associated with **brushes are eliminated**. For example, **brushes tend to produce RFI** (radio-frequency interference) and the **sparking associated** with them is a potential source of **ignition in inflammable atmospheres**. These problems should not be overstated, however. RFI at least has the advantage of high frequency, **so that filter components need not be very large**. This is not necessarily the case with the lower-order harmonics associated with the commutation of the brushless motor. **Commutator motors are quite commonly immersed in automobile petrol tanks to drive the fuel pump**. This shows that they are not automatically **excluded from 'hazardous' environments**.

The problems that arise with commutator motors are sometimes not so obvious. In some applications the accumulation of **brush debris or dust is a problem**, particularly if it gets into the bearings or if it forms a conducting track **that leads to flashover**. The operation and life of brushes depend on

*factors such as atmospheric conditions*, which may necessitate the use of different *brush grades in the same motor* operating in different climates.

An advantage of the brushless configuration in which the rotor is inside the stator is that *more cross-sectional area is available for the power or 'armature' winding*. At the same time the conduction of heat through the frame is improved. Generally an *increase in the electric loading is possible*, providing a *greater specific torque*. *The efficiency is likely to be higher* than that of a commutator motor of equal size, and the absence of brush friction helps further in this regard.

The absence of commutator and brush gear *reduces the motor length*. This is useful not only as a simple space saving, but also as a *reduction in the length between bearings*, so that for a given stack length the lateral stiffness of the rotor is greater, *permitting higher speeds* or a longer active length/diameter ratio. This is important in *servo-type drives where a high torque/inertia ratio is required*. The removal of the commutator reduces the inertia still further

The brushless configuration **DOES NOT COME WITHOUT SOME DISADVANTAGES**. The two main disadvantages relative to the commutator motor are

- (i) The *need for shaft position sensing* and
- (ii) *Increased complexity in the electronic controller*.

Also, the brushless motor is not necessarily less expensive to manufacture than the commutator motor, which is perhaps slightly more amenable to automated manufacture.

#### **4.5.2 CONSTRUCTION OF BLDC**

##### **STATOR**

The stator of a BLDC motor consists of *stacked steel laminations with windings placed in the slots that are axially cut along the inner periphery*. Traditionally, the stator *resembles that of an induction motor*; however, the windings are distributed in a different manner. Most BLDC motors have *three stator windings connected in star fashion*. Each of these windings is constructed with numerous *coils interconnected to form a winding*. One or more coils are placed in the slots and they are interconnected to make a winding. Each of these windings is *distributed over the stator periphery* to form an *even numbers* of poles.

There are two types of stator windings variants: trapezoidal and sinusoidal motors. This differentiation is made on the basis of the interconnection of coils in the stator windings to give the different types of back Electromotive Force (EMF). As their names indicate, the trapezoidal motor gives a back EMF in trapezoidal fashion and the sinusoidal motor's back EMF is sinusoidal. In addition to the back EMF, the phase current also has trapezoidal and sinusoidal variations in the respective types of

motor. This makes the torque output by a sinusoidal motor smoother than that of a trapezoidal motor. However, this comes with an extra cost, as the sinusoidal motors take extra winding interconnections because of the coils distribution on the stator periphery, thereby increasing the copper intake by the stator windings.

## ROTOR

The rotor is made of permanent magnet and can vary from *two to eight pole pairs* with alternate North (N) and South (S) poles. Based on the required magnetic field density in the rotor, the proper magnetic material is chosen to make the rotor. *Ferrite magnets are traditionally used* to make permanent magnets. As the technology advances, *rare earth alloy magnets* are gaining popularity. The ferrite magnets are less expensive but they have the disadvantage of *low flux density for a given volume*. In contrast, the alloy material has high magnetic density per volume and enables the *rotor to compress* further for the same torque. Also, these alloy magnets improve *the size-to-weight ratio* and give higher torque for the same size motor using ferrite magnets. Neodymium (Nd), Samarium Cobalt (SmCo) and the alloy of Neodymium, Ferrite and Boron (NdFeB) are some examples of rare earth alloy magnets. Continuous research is going on to improve the flux density to compress the rotor further. Figure 4.2 shows cross sections of different arrangements of magnets in a rotor.

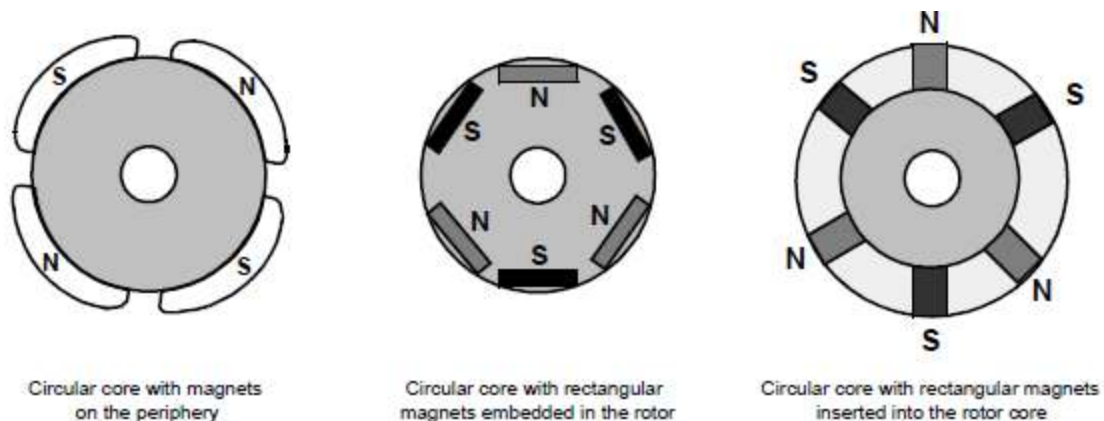


Fig 4.2 Rotor Magnet Cross Sections

## HALL SENSORS

Unlike a brushed DC motor, the commutation of a BLDC motor is controlled electronically. To rotate the BLDC motor, the stator windings should be energized in a sequence. It is important to know the rotor position in order to understand which winding will be energized following the energizing sequence. Rotor position is sensed using Hall effect sensors embedded into the stator. Most BLDC motors have three Hall sensors embedded into the stator on the non-driving end of the motor. Whenever the rotor magnetic poles pass near the Hall sensors, they give a high or low signal, indicating the N or S pole is passing near

the sensors. Based on the combination of these three Hall sensor signals, the exact sequence of commutation can be determined.

Figure 4.3 shows a transverse section of a BLDC motor with a rotor that has alternate N and S permanent magnets and Figure 4.4 shows its cross sectional view. Hall sensors are embedded into the stationary part of the motor. Embedding the Hall sensors into the stator is a complex process because any misalignment in these Hall sensors, with respect to the rotor magnets, will generate an error in determination of the rotor position. To simplify the process of mounting the Hall sensors onto the stator, some motors may have the Hall sensor magnets on the rotor, in addition to the main rotor magnets. These are a scaled down replica version of the rotor. Therefore, whenever the rotor rotates, the Hall sensor magnets give the same effect as the main magnets. The Hall sensors are normally mounted on a PC board and fixed to the enclosure cap on the non-driving end. This enables users to adjust the complete assembly of Hall sensors, to align with the rotor magnets, in order to achieve the best performance. Based on the physical position of the Hall sensors, there are two versions of output. The Hall sensors may be at 60° or 120° phase shift to each other. Based on this, the motor manufacturer defines the commutation sequence, which should be followed when controlling the motor.

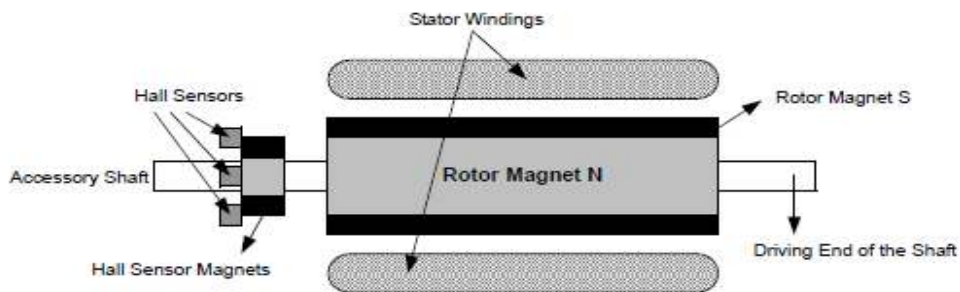


Fig 4.3 BLDC Motor Transverse Section

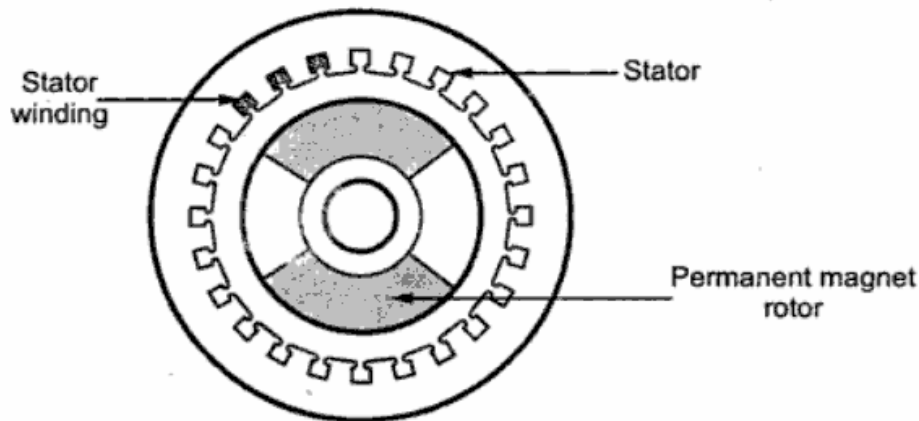


Fig 4.4 Cross Sectional View of BLDC Motor

### 4.5.3 PRINCIPLE OF OPERATION

The brushless DC motor differs from the normal DC motor in that it employs electrical commutation of the armature current rather than the mechanical commutation. The word brushless is used to define the combination of motor, its electronic drive circuit and rotor position sensor. The electronic drive is an inverter which consists of IGBT's, which feeds stator windings. The IGBT's are controlled by pulses generated by rotor position sensors. This ensures that rotor revolves at angular speed which is equal to the average speed of the field produced by the stator.

Like a DC motor the driver circuit is fed from a DC supply. The stator and rotor fields remains stationary with respect to each other at all the speeds. The torque speed characteristic is similar to a DC motor. The speed can be controlled by controlling the input dc voltage. Because of these similarities and as it does not have brushes, it is known as brushless DC motor.

There are two types of Brushless DC motor available in practice they are

- ✓ Unipolar brushless DC motor
- ✓ Bipolar brushless DC Motor.

#### 4.5.3.1 Unipolar Brushless DC motor

In this type the rotor consists of optical sensor. The optical sensor has a light source, three photo transistors  $P_1$ ,  $P_2$  and  $P_3$  mounted on the end plate of the motor, separated by 120 degree from each other and a revolving shutter coupled to the shaft of the motor. The optical sensor is shown in the figure 4.5.

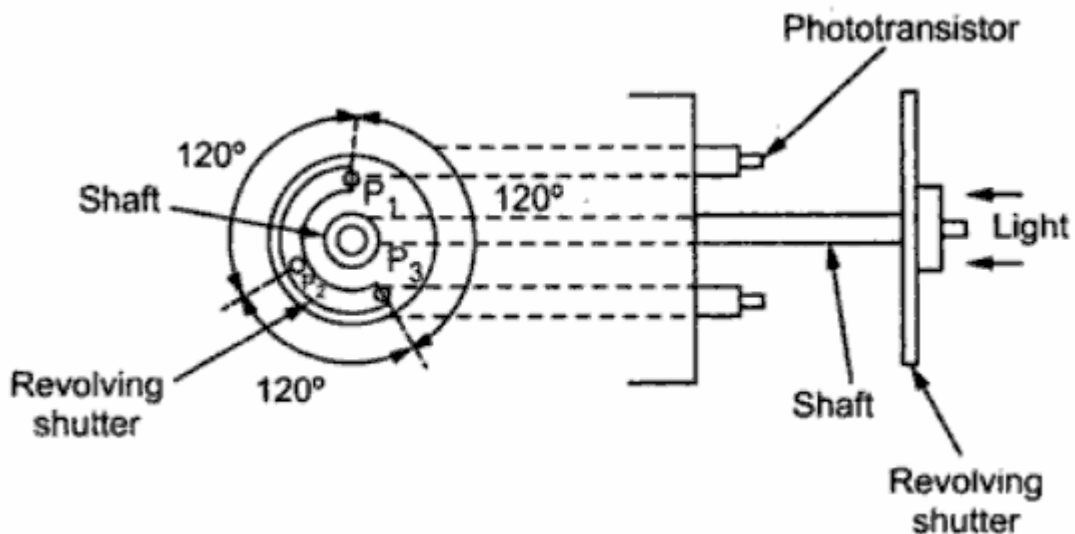


Fig 4.5 Arrangement of an optical sensor.

The stator consists of a three pole stator winding and a two pole rotor consisting of permanent magnets. The driving circuit consists of three transistors  $Q_1$ ,  $Q_2$  and  $Q_3$  used to excite the stator windings. The arrangement is shown in figure 4.6

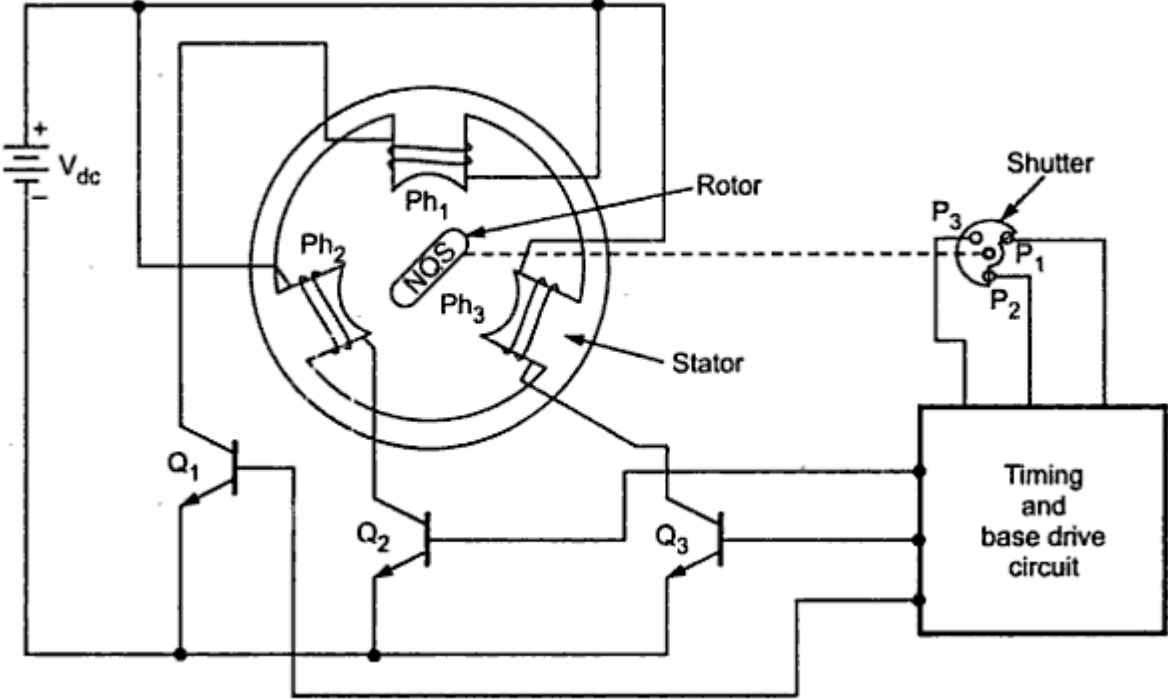


Fig 4.6 Schematic arrangement of Unipolar Brushless DC motor

When the shutter revolves, the phototransistor gets exposed to the light in the sequence of their numbers. In each revolution, the phototransistors generate the pulses  $Pl_1$ ,  $Pl_2$  and  $Pl_3$  which have duration and displacement of 120 degrees. This is shown in figure 4.7.

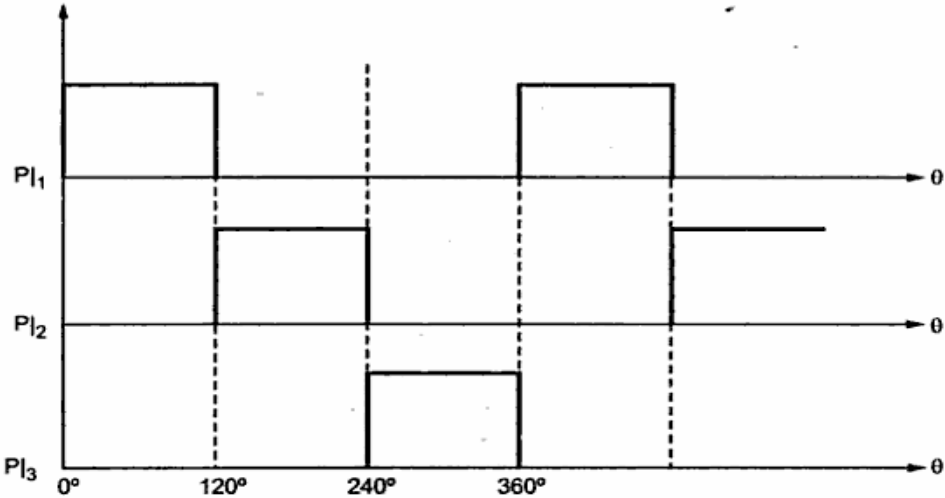


Fig 4.7. Pulses generated by photo transistors.

When light falls on the photo transistors  $P_1$ , it generates a pulse and transistors  $Q_1$  gets turned on. Hence current starts flowing through stator winding  $Ph_1$ . This produces North Pole at pole face of  $Ph_1$ . Due to this South Pole gets attracted towards it and reaches the axis of pole face of  $Ph_1$ . Hence rotor revolves in anticlockwise direction. During this mean time, the light stops falling on  $P_1$  and starts falling of  $P_2$ . Hence Pulse  $Pl_2$  is generated which turns on the transistor  $Q_2$ . So current now starts flowing through stator winding  $Ph_2$ , producing North Pole. Hence rotor further rotates in anticlockwise direction. So the rotor reaches the axis of the pole face of  $Ph_2$ . In the mean time the light stops falling on  $P_2$  and starts falling of  $P_3$ . This causes transistor  $Q_3$  to turn on which produces North Pole at the pole face of  $Ph_3$ . This rotates the rotor further in anticlockwise direction. Switching sequence repeats and continuous rotation of rotor is obtained.

The torque reversal cannot be obtained just by reversing the DC supply as in the case of a conventional DC motor. It can be achieved by operating the timing and base drive circuit in such a way that the transistors  $Q_1$ ,  $Q_2$  and  $Q_3$  conduct for the duration of the pulses  $Pl_2$ ,  $Pl_3$  and  $Pl_1$  respectively. The torque reversal can also achieved by shifting the base drive signals of the transistors by 180 degrees.

This circuit does not use any feed back or freewheeling diodes. This is satisfactory for small motors. In small motors, the inductive energy in the phase windings is very small, to cause any destruction to the transistors. The cost of this motor is low and drive circuit is simple. The main limitation of this motor is that it can not be used for power levels above 100 watts. In large power levels, the stored energy in the phase winding inductance is large and hence feedback diodes are necessary, in such cases bipolar brushless DC motors are used.

#### **4.5.3.2 Bipolar Brushless DC motor**

When a three-phase (brushless) motor is driven by a three-phase bridge circuit, the efficiency, which is the ratio of the mechanical output power to the electrical input power, is the highest, since in this drive an alternating current flows through each winding as an ac motor. This drive is often referred to as 'bipolar drive'. Here, 'bipolar' means that a winding is alternatively energised in the south and north poles.

The rotor uses Hall Effect sensors to sense the position. In fact three Hall Effect sensors and a magnet ring form a rotor position sensor. The Hall sensors are 120 degree electrically apart from each other. Magnet ring is mounted on the rotor shaft and revolves with the rotor. The bipolar brushless DC motor is shown in the figure 4.8.

We shall now survey the principle of the three-phase bridge circuit of Fig.4.8. Here too, we use the optical method for detecting the rotor position; six phototransistors are placed on the end-plate at equal intervals. Since a shutter is coupled to the shaft, these photo elements are exposed in sequence to the light emitted



from a lamp placed in the left of the figure. Now the problem is the relation between the ON/OFF state of the transistors and the light detecting phototransistors. The simplest relation is set when the logic sequencer is arranged in such a way that when a phototransistor marked with a certain number is exposed to light, the transistor of the same number turns ON. Fig.4.8 shows that electrical currents flow through Tr1, Tr4, and Tr5, and terminals U and W have the battery voltage, while terminal V has zero potential. In this state, a current will flow from terminal U to V, and another current from W to V as illustrated in Fig.4.9. We may assume that the solid arrows in this figure indicate the directions of the magnetic fields generated by the currents in each phase. The fat arrow in the centre is the resultant magnetic field in the stator.

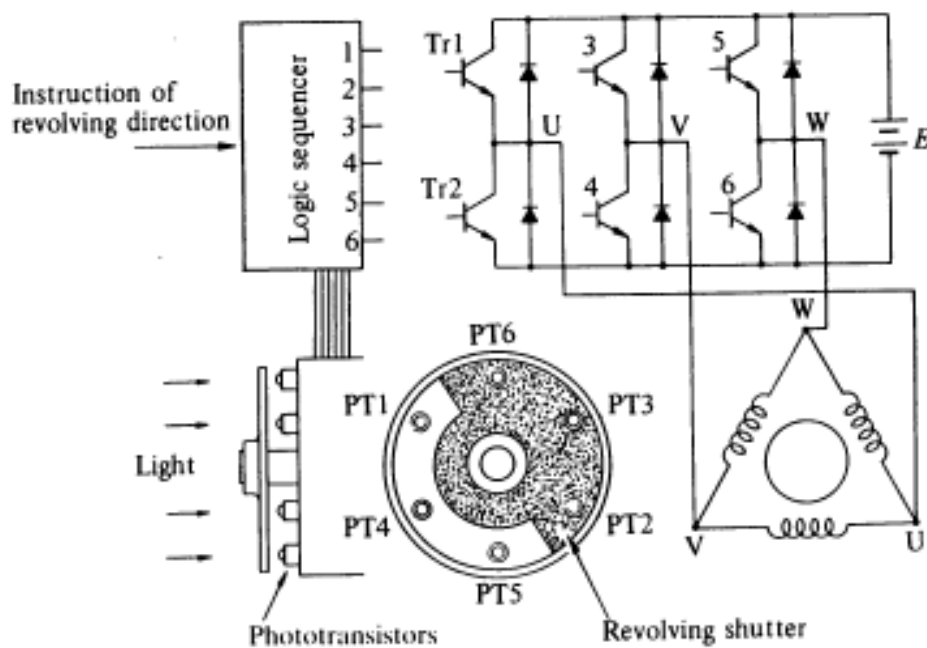


Fig.4.8 Three phase bipolar-driven brushless motor

The rotor is placed in such a position that the field flux will have a  $90^\circ$  angle with respect to the stator's magnetic field as shown in figure.4.9. In such a state a clockwise torque will be produced on the rotor. After it revolves through about  $30^\circ$ , PT5 is turned OFF and PT6 ON which makes the stator's magnetic pole revolves  $60^\circ$  clockwise. Thus when the rotor's south pole gets near, the stator's south pole goes away further to create a continuous clockwise rotation. The ON-OFF sequence and the rotation of the transistor are shown in figure 4.10.

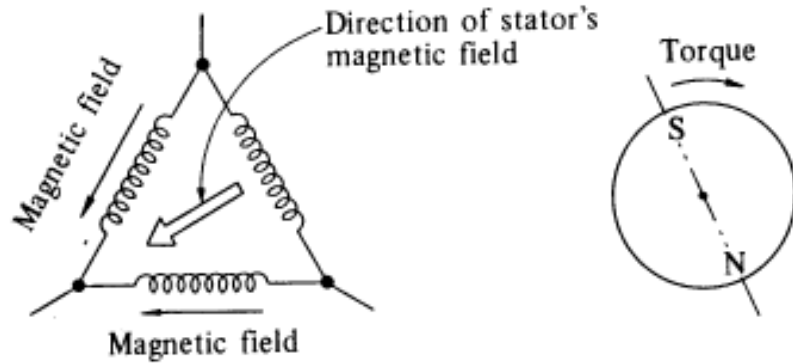


Fig.4.9 Stator's magnetic field in the shutter state of Fig.6, and the direction of torque

Tr 1	1	1	1	0	0	0
2	0	0	0	1	1	1
3	0	0	1	1	1	0
4	1	1	0	0	0	1
5	1	0	0	0	1	1
6	0	1	1	1	0	0

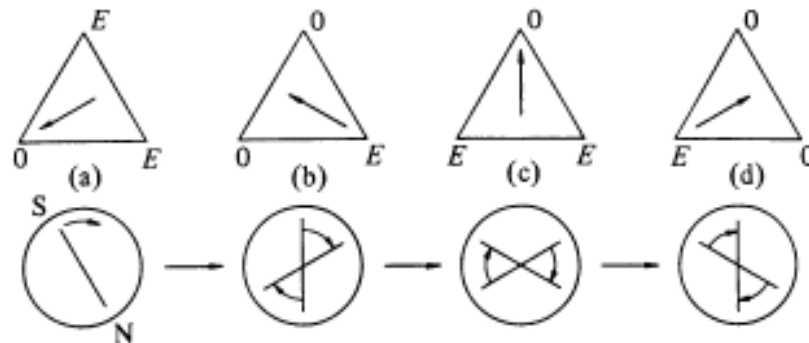


Fig.4.10 Clockwise revolutions of the stator's magnetic field and rotor

The rotational direction may be reversed by arranging the logic sequencer in such a way that when a photo detector marked with a certain number is exposed to light, the transistor of the same number is turned OFF. On the other hand, when a phototransistor is not exposed to light, the transistor of the same number is turned ON. In the positional state of Figure.4.8, Tr2, 3, and 6 are ON, and the battery voltage E appears at terminal V, while U and W have zero electric potential. Then, as shown in figure.4.11 (a), the magnetic field in the stator is reversed, and the rotor's torque is counter-clockwise. After the motor revolves about 30°, Tr2 turns OFF and Tr1 turns ON. At this point, the field has revolved 60° and becomes as shown in (b). As the rotor produces another counterclockwise torque, the counter-clockwise motion continues and the field becomes as shown in (c). This action is repeated in the sequence of (a)→(b)→(c)→(d)..... to produce a continuous counter-clockwise motion.

ON-OFF sequence	1	2	3	4	5	6
Tr 1	0	1	1	1	0	0
2	1	0	0	0	1	1
3	1	1	0	0	0	1
4	0	0	1	1	1	0
5	0	0	0	1	1	1
6	1	1	1	0	0	0

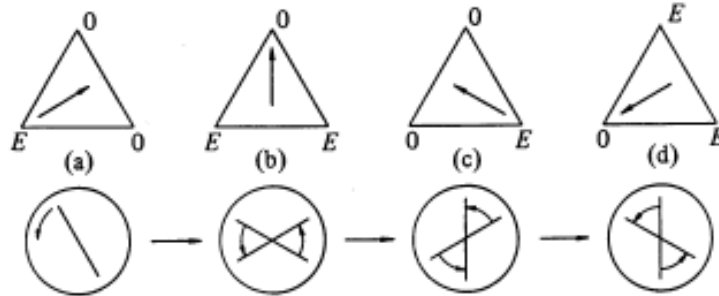


Fig.4.11 Counter-clockwise revolutions of the stator's magnetic field and rotor

#### 4.6 MAGNETIC CIRCUIT ANALYSIS ON OPEN-CIRCUIT

Figure 4.12(a) shows the cross section of a two-pole brushless d.c. motor having high-energy rare-earth magnets on the rotor. The demagnetization curve of the magnet is shown in Fig. 4.12(b). The axial length of both the stator and the rotor is  $l = 50$  mm. First we will consider the open-circuit case that is with no stator current.

Whenever magnetic circuits are used to analyse a magnetic field, the first task is to identify the main flux paths and assign reluctances or permeances to them. The brushless D.C. motor is very amenable to this kind of analysis. The left half of Fig. 4.12(a) shows the expected flux pattern and Fig. 4.12(c) shows the equivalent magnetic circuit. Only half of the equivalent circuit is shown in Fig. 4.12(c); the lower half is the mirror-image of the upper half about the horizontal axis, which is an equipotential. It is of course permissible to simplify the circuit in this way only if the two halves are balanced. If they are not, the horizontal axis might still be an equipotential but the fluxes and magnetic potentials in the two halves would be different, and there could be residual flux in the axial direction, i.e. along the shaft. In practice axial flux is undesirable because it can induce current to flow in the bearings; in some cases this results in accelerated wear. In the following, the steel core of the stator and the rotor shaft are assumed to be infinitely permeable. Each magnet is represented by a 'Norton' equivalent circuit consisting of a flux generator in parallel with an internal leakage permeance (Fig. 4.12(c))

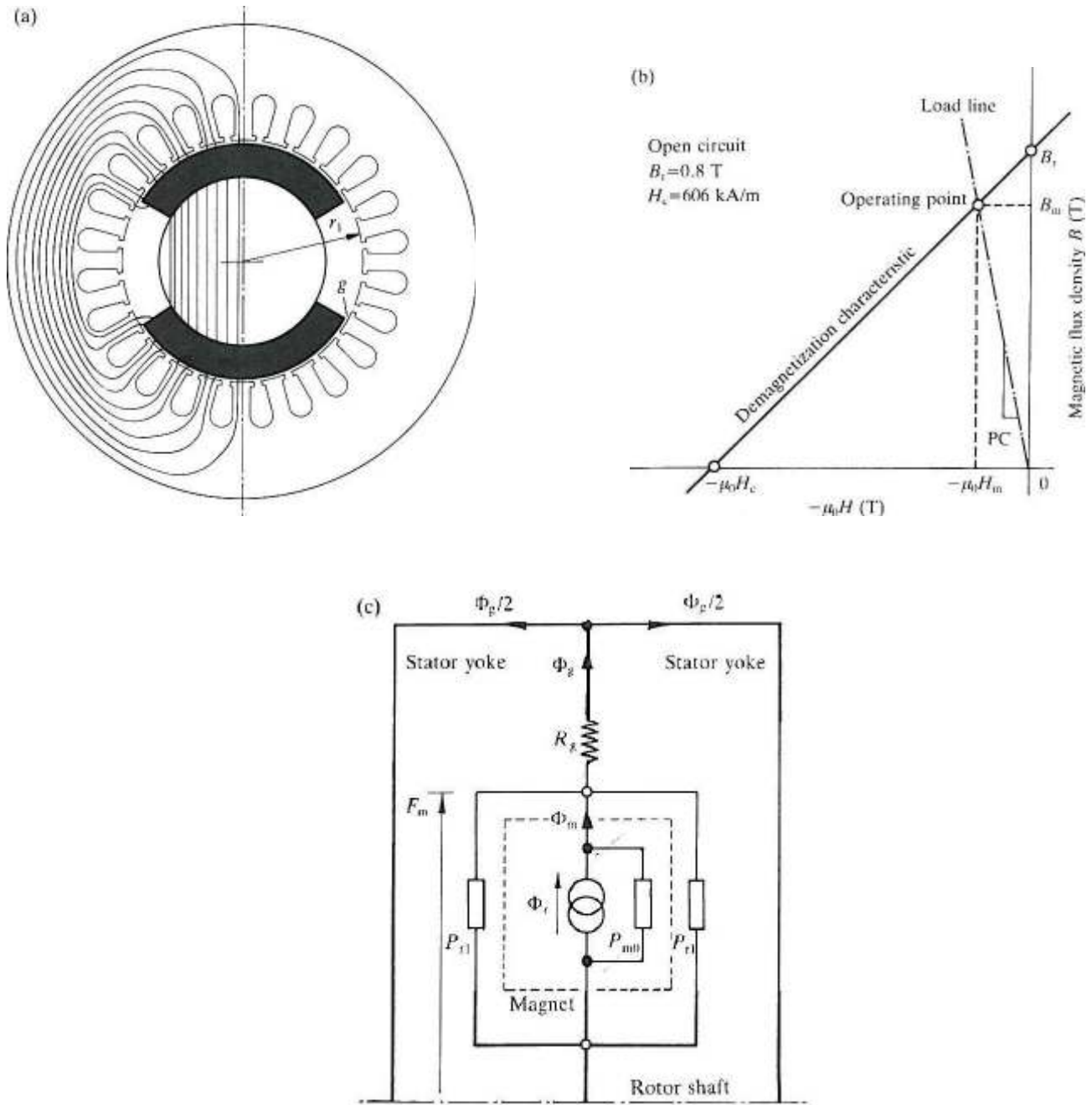


Fig. 4.12. Simple magnetic circuit analysis of BLDC motor, (a) Motor cross section and flux pattern, (b) Magnet demagnetization curve, (c) Magnetic equivalent circuit.

$$\phi_r = B_r A_m; P_{mo} = \frac{\mu_0 \mu_{rec} A_m}{l_m} \text{-----} (4.1)$$

Where  $A_m$  is the pole area of the magnet;  $l_m$  is the magnet length in the direction of magnetization (in this case its radial thickness); and  $B_r$  is the remanent flux-density.  $\mu_{rec}$  is the relative recoil permeability, that

is, the slope of the demagnetization curve divided by  $\mu_0$ ). In this case the outer pole area is larger than the inner pole area, but to keep the analysis simple we will take the average. With a magnet arc of 120 degrees,

$$A_m = \frac{2}{3} \pi \left( r_1 - g - \frac{l_m}{2} \right) l \quad (4.2)$$

Most of the magnet flux crosses the air gap via the air gap reluctance  $R_g$

$$R_g = \frac{g'}{\mu_0 A_g} \quad (4.3)$$

Where  $g'$  is the equivalent air gap length allowing for slotting. The slotting can be taken into account by means of Carter's coefficient, in which case

$$g' = K_c g \quad (4.4)$$

The air gap area  $A_g$  is the area through which the flux passes as it crosses the gap. The precise boundary of this area is uncertain because of fringing, both at the edges of the magnet and at the ends of the rotor. An approximate allowance for fringing can be made by adding  $g$  at each of the four boundaries, giving

$$A_g = \left[ \frac{2}{3} \pi \left( r_1 - \frac{g}{2} \right) + 2g \right] (l + 2g) \quad (4.5)$$

The remaining permeance in the magnetic circuit is the rotor leakage permeance  $P_{rl}$ , which represents the paths of magnet flux components that fail to cross the air gap. The rotor leakage permeance is difficult to estimate because the flux paths are not obvious. An accurate evaluation of rotor leakage is possible only with numerical techniques such as the finite-element method. With the configuration shown, the rotor leakage permeance is quite small, typically 5-20 per cent of the magnet internal permeance, and it is convenient to include it in a modified magnet internal permeance by writing

$$P_m = P_{mo} + P_{rl} = P_{mo} (1 + P_{rl}) \quad (4.6)$$

Where  $p_{rl}$  is the normalized rotor leakage permeance, i.e., normalized to  $P_{mo}$

The magnetic circuit can now be solved. Equating the m.m.f. across the magnet to the m.m.f. across the air gap,

$$F_m = \frac{(\Phi_r - \Phi_g)}{P_m} = \Phi_g R_g, \Phi_g = \frac{\Phi_r}{(1 + P_m R_g)} \quad (4.7)$$

If we write the ratio of magnet pole area to air gap area as

$$C_{\Phi} = \frac{A_m}{A_g} \text{-----(4.8)}$$

Then the air gap flux-density can be extracted as

$$B_g = \frac{C_{\Phi}}{(1 + P_m P_g)} B_r \text{-----(4.9)}$$

The magnet flux-density  $B_m$  can be derived by a similar process

$$B_m = \frac{1 + P_{r1} R_g}{(1 + P_m P_g)} B_r \text{-----(4.10)}$$

Now that we know the magnetic flux-density, it is easy to solve for the magnetizing force  $H_m$  in the magnet using the demagnetization characteristic, Fig. 4.12(b). Mathematically the result is

$$-H_m = \frac{B_r - B_m}{\mu_0 \mu_{rec}} A / m \text{-----(4.11)}$$

The negative sign signifies a demagnetizing force and indicates that the magnet operates in the second quadrant of the  $B$ - $H$  curve, as expected.

The line drawn from the origin through the operating point in Fig. 4.12(b) is called the 'load-line' and the absolute value of its slope, normalized to  $\mu_0$ , is called the 'permeance coefficient', PC. The following formula can be derived for PC

$$PC = \mu_{rec} \frac{1 + P_{r1} R_g}{P_{m0} R_g} \text{-----(4.12)}$$

Alternatively, in terms of geometric dimensions

$$PC = \frac{1 + P_{r1} \mu_{rec} C_{\Phi} \frac{g'}{l_m}}{C_{\Phi} \frac{g'}{l_m}} \text{-----(4.13)}$$

If Fig. 4.12(b) is drawn with  $\mu_0 H_m$  along the x-axis instead of  $H_m$ , then the units of both axes are the same (T) and the permeance coefficient is the actual slope of the load line.

The permeance coefficient is useful as a measure of how far down the demagnetization curve the magnet operates on open-circuit. It can be shown that

$$\frac{B_m}{B_r} = \frac{PC}{PC + \mu_{rec}} \text{-----(4.14)}$$

In motors with a weak flux-concentration factor, the magnet should operate on open-circuit at a high permeance coefficient to maximize the air gap flux-density and the torque per ampere, and to provide adequate margin against demagnetization by armature reaction. Surface-magnet motors generally do have a weak flux concentration factor and a permeance coefficient of six or more is quite normal when using 'hard' magnets.

The air gap flux-density on open-circuit is plotted in Fig. 4.13. In practice, because of fringing, the distribution is not perfectly rectangular, and there are circumferential as well as radial components of  $B$  at the edges of the magnets. Because of the slotting of the stator bore, there will in general be an appreciable ripple superimposed on the calculated waveform. The detailed analysis of all these effects requires a numerical method such as the finite-element method.

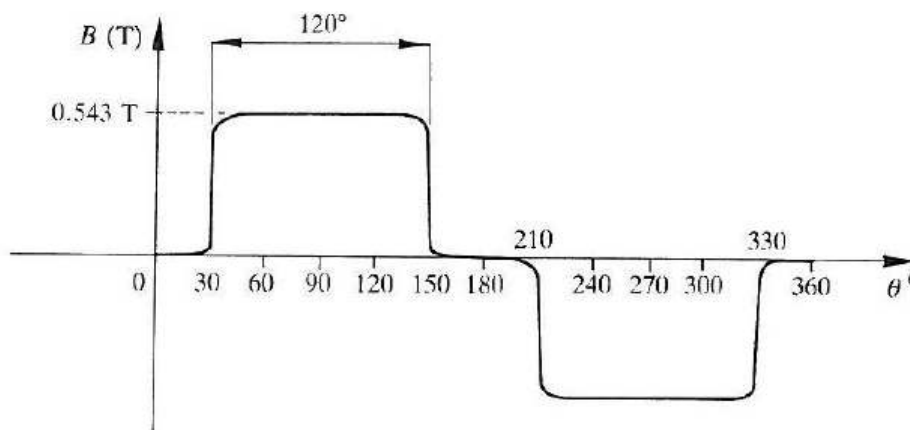


FIG. 4.13. Air gap flux-density on open circuit.

#### **4.7 BRUSHLESS DC MOTOR: TORQUE AND E.M.F. EQUATIONS**

The basic torque and e.m.f. equations of the brushless D.C. motor are quite simple, and resemble those of the D.C. commutator motor. The following derivation attempts to encompass several fundamental aspects of these two equations, so as to lay a foundation for understanding the control characteristics and limitations, and the similarities and differences with other machines.

A simple 'concept machine' is shown in Fig. 4.14(a). Note that the two-pole magnet has a pole arc of 180 degrees, instead of the 120 degrees analysed in the previous section. The air gap flux-density waveform is ideally a square wave as shown in Fig. 4.14(b). In practice, fringing causes the corners to be somewhat rounded. The coordinate axes have been chosen so that the centre of a north pole of the magnet is aligned with the x-axis, i.e. at  $\theta = 0$ .

The stator has 12 slots and a three-phase winding. Thus there are two slots per pole per phase. Each phase winding consists of two adjacent full-pitch coils of  $N_1$  turns each, whose axes are displaced from one another by 30 degrees. The winding is a single-layer winding, and any slot contains  $N_1$  conductors from only one phase winding. This winding is equivalent, in the active length, to a degenerate concentric winding with only one coil per pole per phase, having a fractional pitch of 5/6. This is a more practical winding than the one analysed because it has less bulky end windings and is generally easier to assemble. For the same reason, its copper losses are lower.

Consider the flux-linkage  $\psi_1$  of coil  $a_1A_1$  as the rotor rotates. This is shown in Fig. 4.14(c). Note that  $\theta$  now represent the movement of the rotor from the reference position in Fig. 4.14(a). The flux-linkage varies linearly with rotor position because the air gap flux-density set up by the magnet is constant over each pole-pitch of the rotor. Maximum positive flux-linkage occurs at 0 and maximum negative flux-linkage at 180°. By integrating the flux-density around the air gap, the maximum flux-linkage of the coil can be found as

$$\psi_{1\max} = N_1 \int B(\theta) r_1 d\theta l = N_1 B_g \pi r_1 \quad \text{----- (4.15)}$$

and the variation with  $\theta$  as the rotor rotates from 0 to 180° is given by

$$\psi_1(\theta) = \left[ 1 - \frac{\theta}{\pi/2} \right] \psi_{1\max} \quad \text{----- (4.16)}$$

The e.m.f. induced in coil  $a_1A_1$  is given by

$$e_1 = -\frac{d\Psi_1}{dt} = -\frac{d\Psi_1}{d\theta} \frac{d\theta}{dt} = -\omega \frac{d\Psi_1}{d\theta} \quad \text{----- (4.17)}$$

This gives

$$e_1 = 2N_1 B_g l r_1 \omega [\text{Volts}] \quad \text{----- (4.18)}$$

Fig. 4.14(d). Note that the waveform of e.m.f. in this full-pitch coil with respect to time is an exact replica of the flux-density waveform with respect to position around the rotor in Fig. 4.14(b).

The e.m.f. induced in the second coil of phase A is identical, but retarded in phase by 30°. This is shown in Fig. 4.14(e). If the two coils are connected in series, the total phase voltage is the sum of the two separate coil voltages, and this is shown in Fig. 4.14(f). The basic effect of distributing the winding into two coils is to produce a stepped e.m.f. waveform. In practice, fringing causes its corners to be rounded, as shown by the dotted lines. The waveform then has the 'trapezoidal' shape that is characteristic of the brushless D.C. motor. With 180° magnet arcs and two slots per pole per phase, the flat top of this waveform is ideally 150° wide, but in practice the fringing field reduces this to a somewhat smaller value, possibly as little as 120°.



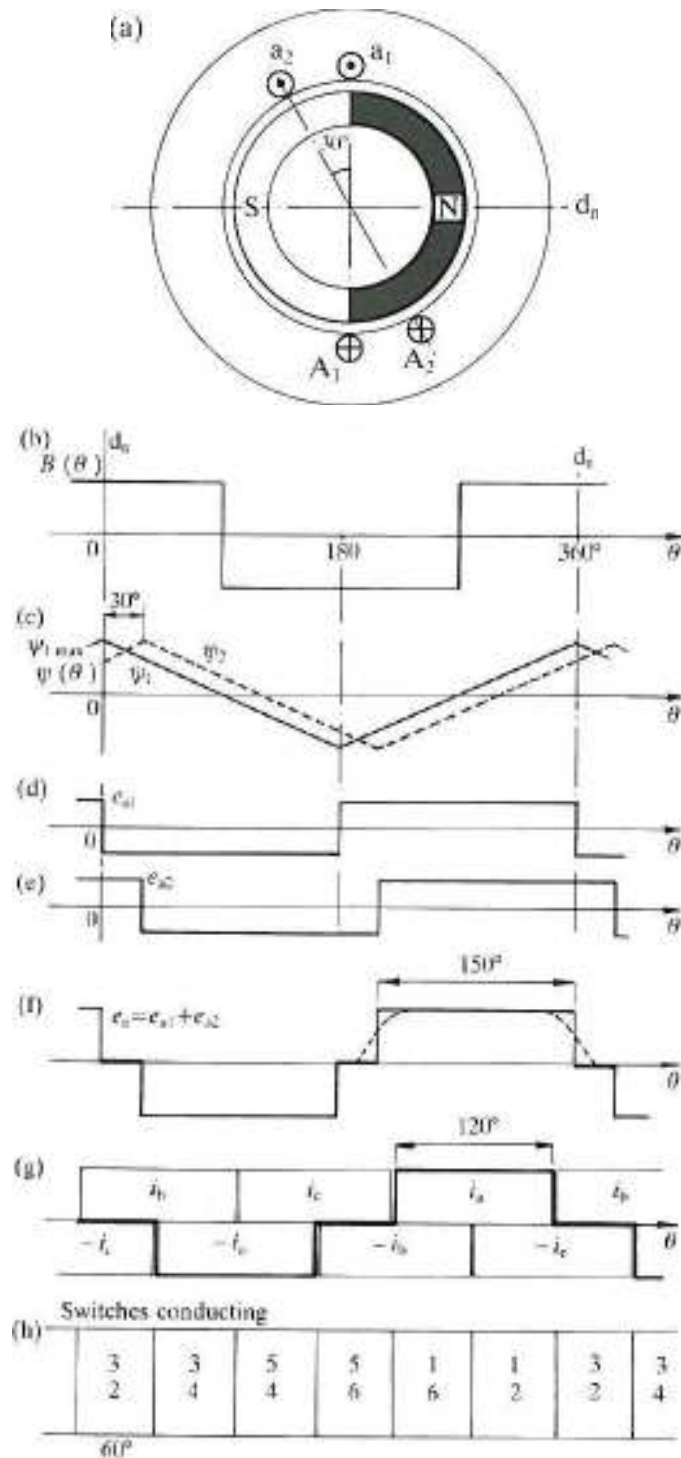


FIG. 4.14. Brushless D.C. motor with ideal waveforms of flux-density, e.m.f., and current, (a) Motor showing two coils of one phase, (b) Magnet flux-density around the air gap. (c) Flux-linkage of coils 1 and 2 as the rotor rotates, (d) e.m.f. waveform of coil 1. (e) e.m.f. waveform of coil 2. (f) e.m.f. waveform of phase a. (g) Ideal phase current waveforms, (h) Switching pattern of switches

The magnitude of the flat-topped phase e.m.f. is given by

$$e_1 = 2N_{ph}B_g l r_1 \omega [\text{Volts}] \text{-----} (4.19)$$

Where  $N_{ph}$  is the number of turns in series per phase. In this case

$$N_{ph} = 2N_1 \text{-----} (4.20)$$

because the two coils considered are assumed to be in series. In a machine with  $p$  pole-pairs, the equation remains valid provided  $N_{ph}$  is the number of turns in series per phase and  $\omega$  is in mechanical radians per second.

Figure 4.14(g) shows an ideal rectangular waveform of phase current, in which the current pulses are 120 electrical degrees wide and of magnitude  $I$ . The positive direction of current is against the e.m.f., that is, positive current is motoring current. The conduction periods of the three phases are symmetrically phased so as to produce a three-phase set of balanced 120° square waves. If the phase windings are star-connected, as in Fig. 4.15(a), then at any time there are just two phases and two transistors conducting.

During any 120° interval of phase current the instantaneous power being converted from electrical to mechanical is

$$P = \omega T_e = 2eI \text{-----} (4.21)$$

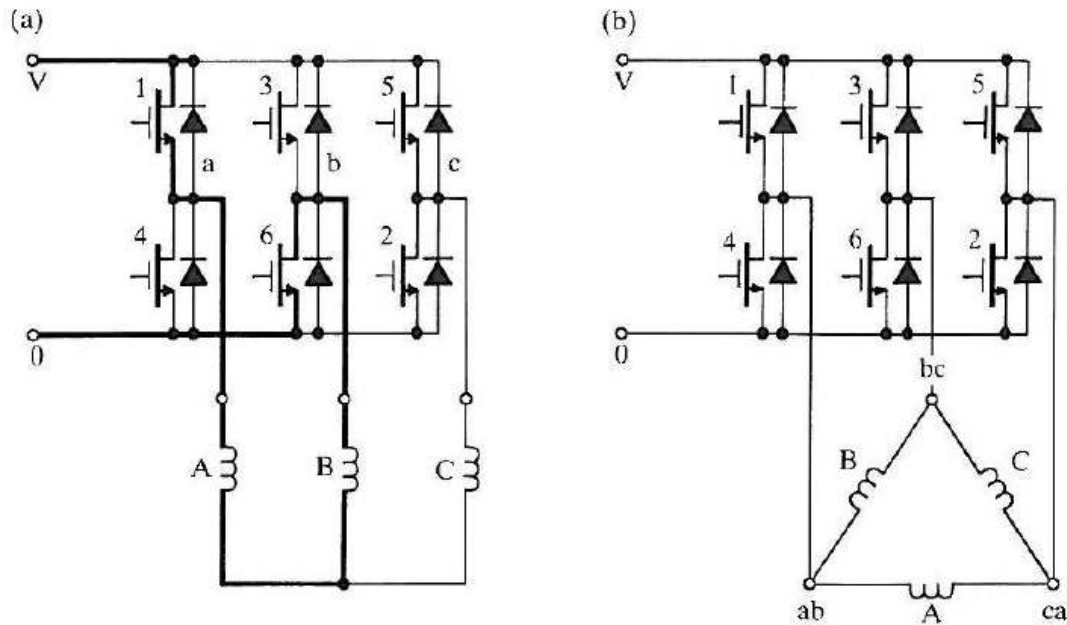


Fig 4.15 Converter or Inverter of BLDC motor (a) With star connected Phase Winding (b) With Delta Connected Phase Winding

The '2' in this equation arises from the fact that two phases are conducting. Using the expression derived above for the e.m.f., the electromagnetic torque is given by

$$T_e = 4N_{ph}B_g l r_1 I [Nm] \text{-----} (4.22)$$

This equation is valid for any number of pole-pairs. The similarity between the brushless motor and the commutator motor can now be seen. Writing  $E=2e$  to represent the combined e.m.f. of two phases in series, the e.m.f. and torque equations can be written in the form

$$E = K\Phi\omega \text{ and } T = K\Phi I \text{-----} (4.23)$$

Where  $K = 4N_{ph}$  and  $\Phi = B_g r_1 \pi l$

$k$  is the 'armature constant' and  $\Phi$  is the flux. These equations for e.m.f. and torque are exactly the same as for the D.C. commutator motor; only the form of the constant  $k$  is different. It is clear that with ideal wave shapes and with perfect commutation, these equations are true at all instants of time. The electronic commutation of the converter switches has thus assumed the function of the mechanical commutator in the commutator motor, to give a pure 'd.c.' machine with constant, ripple-free torque.

#### **4.8 TORQUE/SPEED CHARACTERISTICS OF BLDC MOTOR**

The torque/speed curve of the ideal brushless motor can be derived from the foregoing equations. If the commutation is perfect and the current waveforms are exactly as shown in Fig. 4.14(g), and if the converter is supplied from an ideal direct voltage source  $V$ , then at any instant the following equation can be written for the D.C. terminal voltage:

$$V = E + RI \text{-----} (4.24)$$

Where  $R$  is the sum of two phase resistances in series and  $E$  is the sum of two phase e.m.f.s in series. This equation is exactly the same as that of the commutator motor. The voltage drops across two converter switches in series are omitted, but they correspond exactly to the two brush voltage drops in series in the commutator motor.

Using this equation together with the e.m.f. and torque equations, the torque/speed characteristic can be derived as:

$$\omega = \omega_0 \left[ 1 - \frac{T}{T_0} \right] \text{-----} (4.25)$$

Where the no-load speed is

$$\omega_0 = \frac{V}{k\Phi} \text{ rad/sec} \text{-----} (4.26)$$

and the stall torque is given by

$$T_0 = k\Phi I_0 \text{-----} (4.27)$$

This is the torque with the motor stalled, i.e. at zero speed. The stall current is given by

$$I_0 = \frac{V}{R} \text{-----} (4.28)$$

This characteristic is plotted in Fig. 4.16. If the phase resistance is small, as it should be in an efficient design, then the characteristic is similar to that of a shunt D.C. motor. The speed is essentially controlled by the voltage  $V$ , and may be varied by varying the supply voltage. The motor then draws just enough current to drive the torque at this speed. As the load torque is increased, the speed drops, and the drop is directly proportional to the phase resistance and the torque.

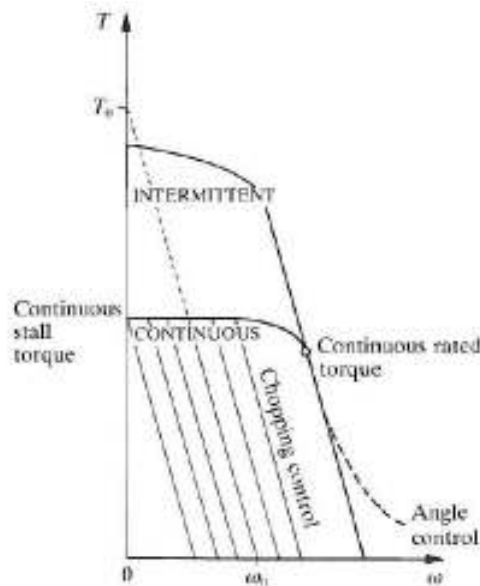


Fig 4.16 Torque/speed characteristic of ideal brushless D.C. motor.

### **4.5 BLDC MOTOR CONTROLLERS**

The general structure of a controller for a brushless PM motor is shown in Fig. 4.17. This schematic diagram shows the functions required to control the drive in the 'chopping control' range of Fig. 4.16, i.e., the commutation angles are fixed.

The rotor shaft position is sensed by a Hall-effect sensor, a slotted optical disk, or some other transducer, providing signals as represented in Table 4.1. These signals are 'decoded' by combinatorial logic to provide the firing signals for 120° conduction on each of the three phases. The commutation logic or 'rotor position decoder' therefore has six outputs which control the upper and lower phaseleg

transistors. Programmable logic arrays, gate arrays, and EPROMS are all suitable for this function. In general there will be level-shifting circuits to buffer the outputs of the logic circuit and provide the drive to the power devices.

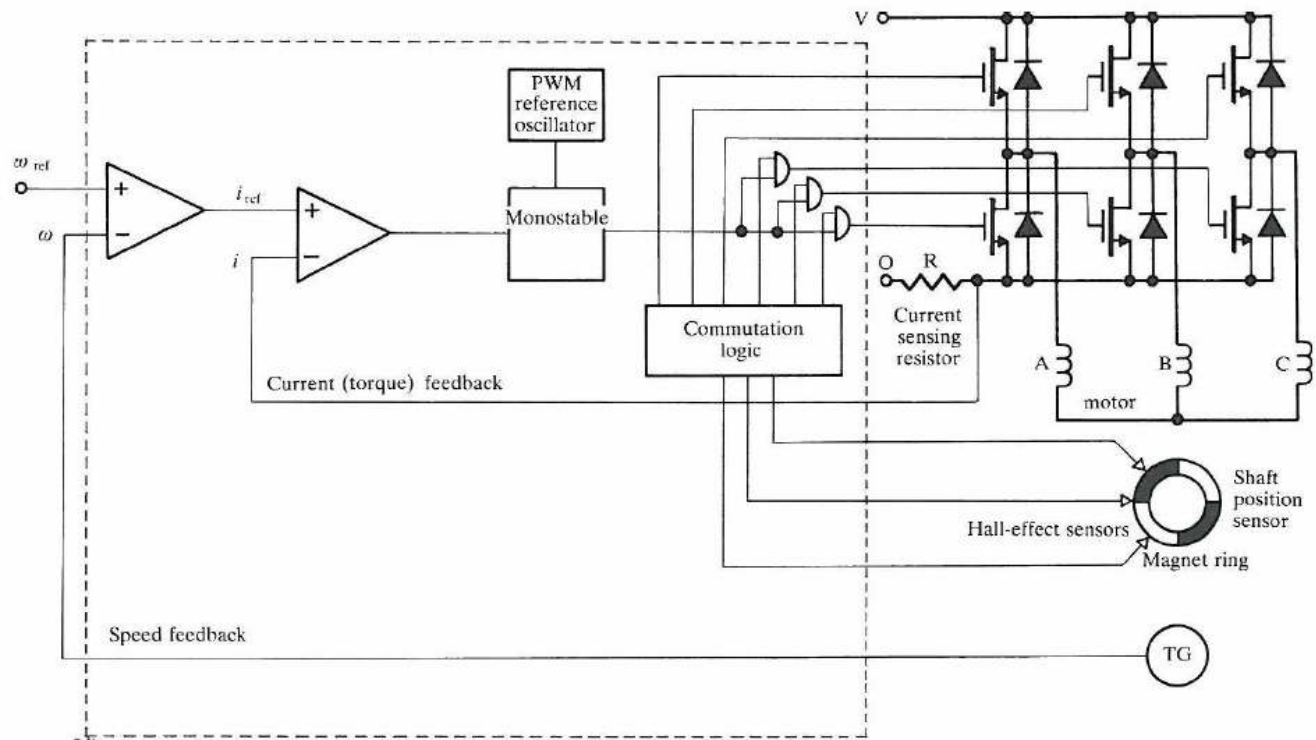


Fig 4.17 Structure of Controllers for PMBLDC motors

The basic forward control loop is a voltage control, implemented in Fig. 4.17 by a mono stable clocked at a fixed reference frequency, which is typically a few kHz. In general it is desirable to make this frequency ultrasonic to minimize noise. The duty-cycle or off-time is controlled by an analogue voltage reference that represents the desired speed. In Fig. 4.17 the p.w.m. is applied only to the lower phase leg transistors. This not only reduces the current ripple but also avoids the need for wide bandwidth in the level-shifting circuit that feeds the upper phase leg transistors. With higher D.C. supply voltages this can be a useful saving. The upper transistors need not be of the same type as the lower ones and need only switch at the commutation frequency, i.e. only a few hundred Hz. Note the use of ANQ gates as a simple way of combining the commutation and chopping signals to the lower transistors. (In practice these would usually be implemented in negative TTL or CMOS logic).

From a control point of view the brushless motor is similar to the D.C. commutator motor, as the simple torque and voltage equations show. Consequently it is possible to implement current (torque) feedback and speed feedback in the same way as for the d.c. motor, and generally this results in a well-behaved

system although compensation may be necessary in either or both loops to improve stability and transient response. A tight speed control is thus possible over a wide range of speed and torque using relatively simple techniques that are familiar with commutator motors. This is in contrast, to some degree, with the a.c. induction motor, which cannot accommodate speed and torque control loops in this form without having reference-frame transformations, as in the field-oriented control technique, or their equivalent.

Sometimes the instantaneous current in the brushless PM motor is regulated in each phase by a hysteresis-type regulator which maintains the current within adjustable limits. This is called 'current-mode' control and several algorithms are possible to control the switching. In this case current sensors are needed in each phase, and their bandwidth must obviously be considerably wider than that of the sensing resistor shown in Fig. 4.17. The speed feedback signal, derived in Fig. 4.17 from a tachometer-generator TG, can also be derived from the shaft position sensor by a frequency-to-voltage converter. This technique only works at high speeds.

Many of the functions of the circuit in Fig. 4.17 can be performed digitally, and it is increasingly common to have a serial communications interface that permits the system to be computer controlled. In high-performance systems the shaft position sensor may be a resolver or optical encoder, with special-purpose decoding circuitry. At this level of control sophistication, it is possible to fine-tune the firing angles and the p.w.m. control as a function of speed and load, to improve various aspects of performance such as efficiency, dynamic performance, or speed range.

There is a wide range of integrated circuits available with many of the functions in Fig. 4.17. The functions inside the dotted line are all found on many such products, as well as many protective functions such as over- and under-voltage protection, over current protection, and lockout protection (preventing the upper and lower switches in one phase leg from turning on at the same time and causing a 'shoot-through' failure).

## **4.6 SINE WAVE PM BRUSHLESS MOTOR DRIVES (PMSM)**

### **4.6.1 CONSTRUCTION**

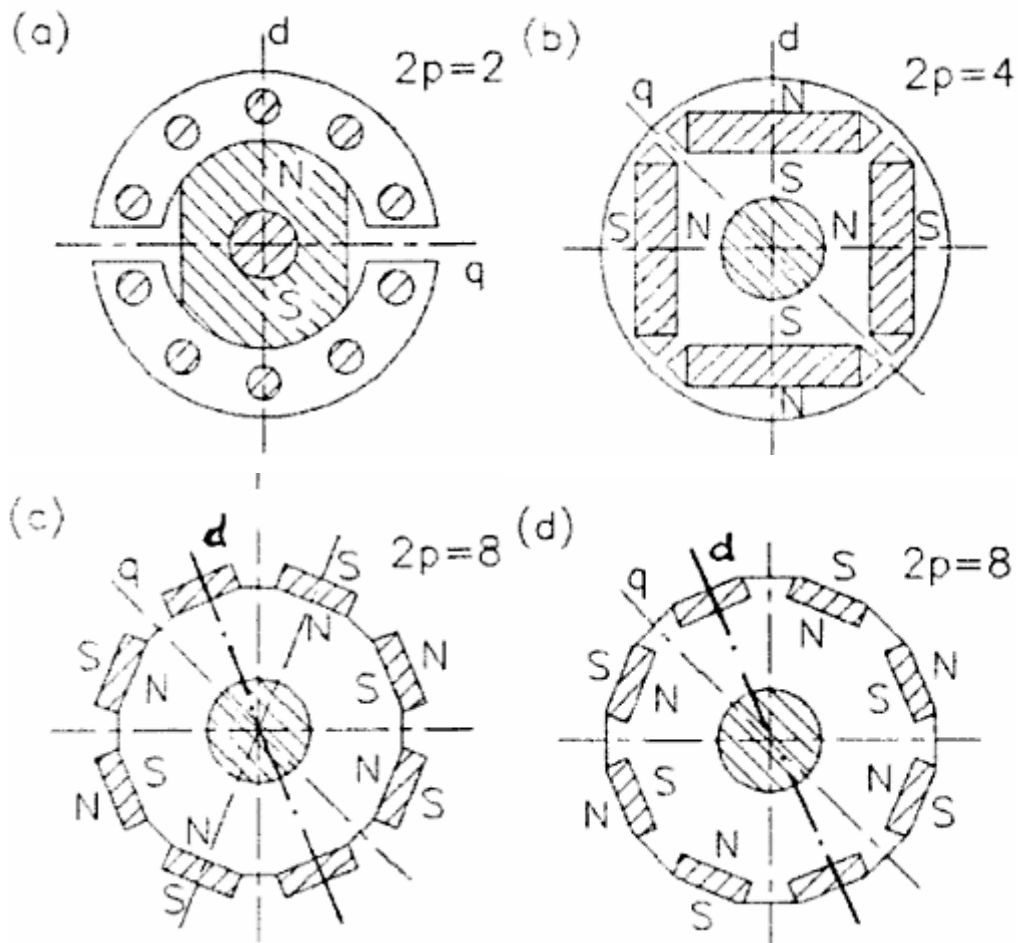
Synchronous motors operate at constant speed in absolute synchronism with the line frequency. Synchronous motors are classified according to their rotor design, construction, materials and operation into the four basic groups.

- ✓ Electromagnetically excited motor
- ✓ PM motors
- ✓ Reluctance motors
- ✓ Hysteresis motor

In electromagnetically excited and PM motors a cage winding is frequently mounted on salient pole rotors to provide asynchronous starting and to damp oscillations under transient conditions, so called damper. Recent development in rare earth PM materials and power electronics have opened new prospects on the design, construction and application of PM synchronous motors.

PM Synchronous motors usually built with one of the following rotor configurations

- ✓ Classical, with salient poles, laminated pole shoes and cage winding (Fig 4.18 a)
- ✓ Interior magnet rotor (Fig 4.18 b,i,j)
- ✓ Surface magnet rotor (Fig 4.18 c,g,h)
- ✓ Inset magnet rotor (Fig 4.18d)
- ✓ Rotors with buried magnet symmetrically distributed (Fig 4.18 e)
- ✓ Rotors with buried magnet asymmetrically distributed (Fig 4.18 f)



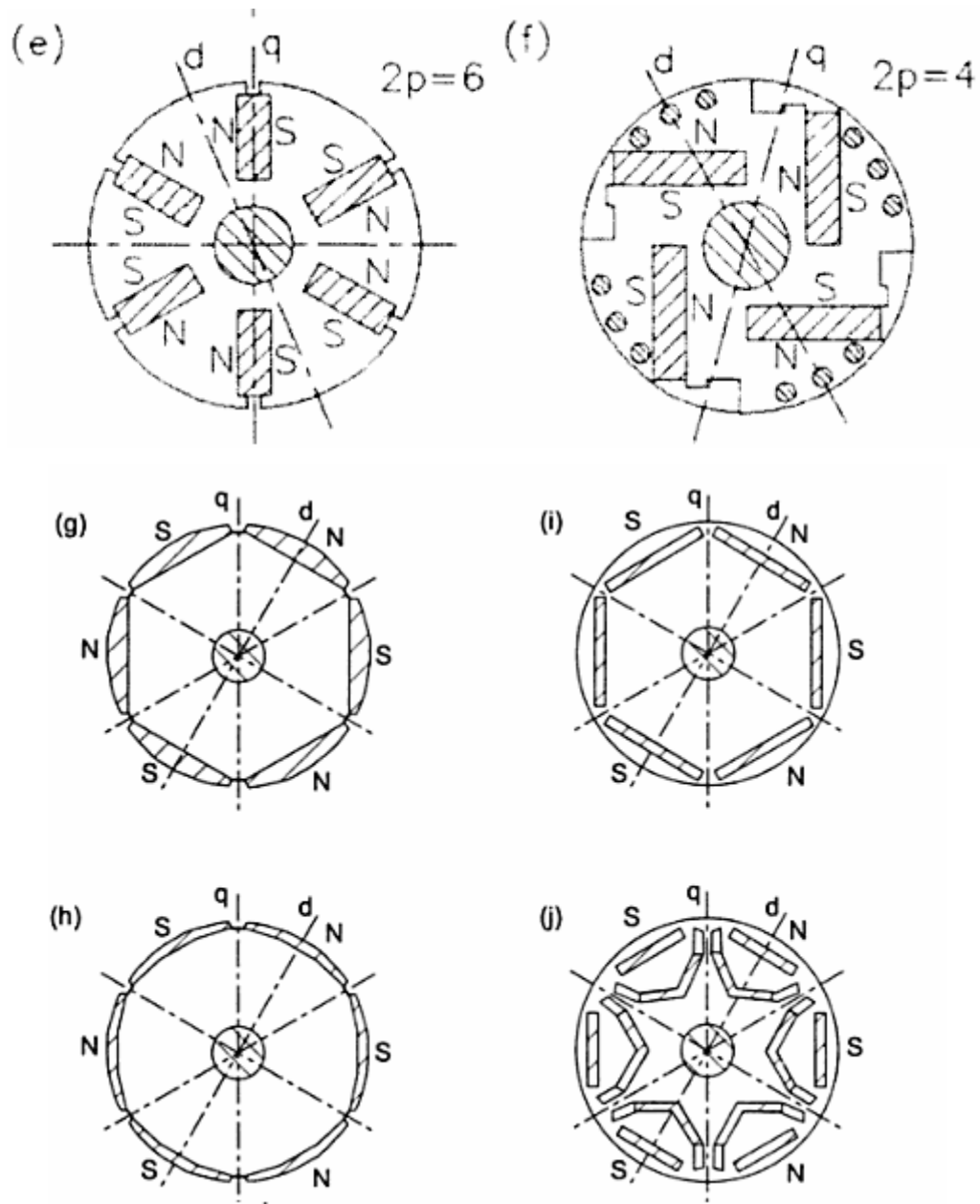


Fig 4.18 Rotor Configurations for PM Synchronous motors

The sine wave motor differs in all three respects. It has:

1. Sinusoidal or quasi-sinusoidal distribution of magnet flux in the air gap;
2. Sinusoidal or quasi-sinusoidal current waveforms;
3. Quasi-sinusoidal distribution of stator conductors; i.e. short-pitched and distributed or concentric stator windings.

#### **4.7 IDEAL SINEWAVE MOTOR: TORQUE AND E.M.F EQUATIONS**

The torque production can be analysed in terms of the interaction of the magnet flux and the stator ampere-conductor distribution, as in the square wave motor. Figure 4.19 shows the basic concept for a



machine with two poles. The stator conductors are distributed as a sine-distributed conductor-density around the stator bore, such that in any angle  $d\theta$  the number of conductors is

$$\frac{N_s}{2} \sin P\theta d\theta \dots \dots \dots (4.29)$$

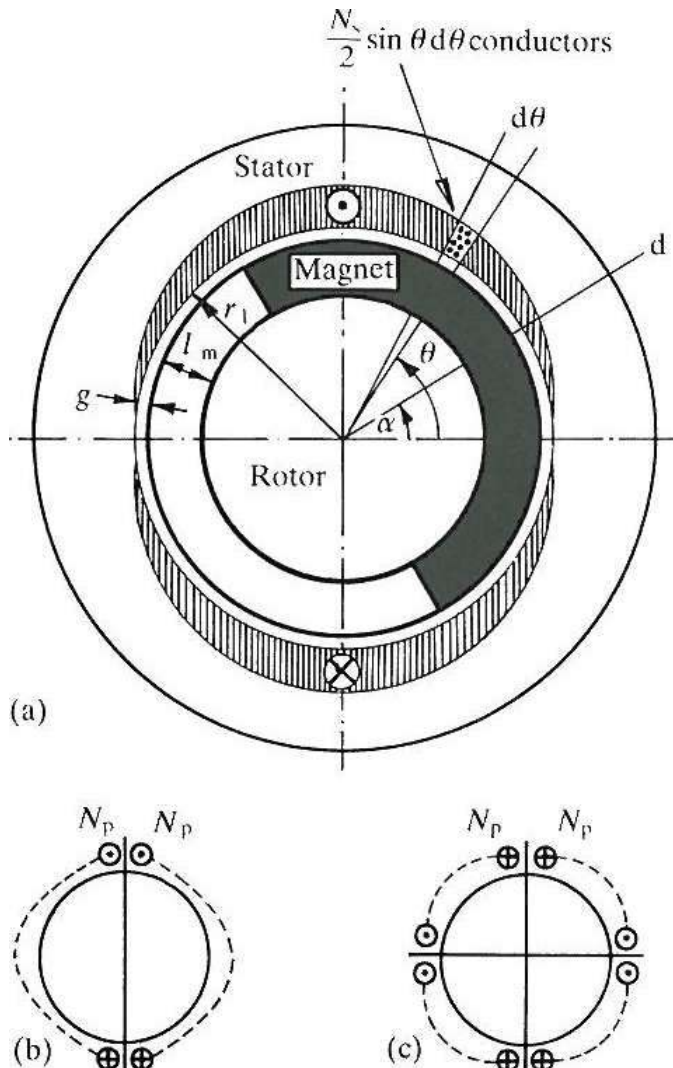


FIG. 4.19. (a) Ideal sine wave brushless motor with pure sine-distributed phase winding and permanent-magnet rotor with sine-distributed flux, (b) Turns/pole for two-pole winding, (c) Turns/pole for four-pole winding.

By integrating this expression over one-half of an electrical pole-pitch, i.e., from 0 to  $\pi/2p$ , and noting that one turn comprises two conductors in series, the number of turns per pole,  $N_p$ , is determined to be

$$N_p = \frac{N_s}{2} \dots \dots \dots (4.30)$$

This means that if all the poles are connected in series,  $N_s$  is automatically equal to the number of turns in series in the whole winding, i.e. the number of turns in series per phase. The poles will be assumed to be

so connected unless it is stated otherwise. The notional distribution of the 'turns per pole' is shown in Fig. 4.19(b) and (c) for two-pole and four-pole motors

In the following analysis the angle  $\theta$  is in mechanical degrees or radians. The stator ampere-conductor distribution is a sine-distributed current sheet of the same form as the conductor distribution, such that in angle  $d\theta$  the ampere-conductors flowing in the positive direction (out of the paper) are

$$i \frac{N_s}{2} \sin P\theta \dots \dots \dots (4.31)$$

The rotor magnet flux distribution is centered on its north d-axis, which is displaced by a positive angle  $\alpha$  from the axis of the stator winding:

$$B(\theta) = \hat{B} \cos(P\theta - \alpha) \dots \dots \dots (4.32)$$

Here  $\alpha$  is expressed in electrical radians, which will prove convenient later. The force on the elementary group of ampere-conductors is in the circumferential direction and is

$$F = \hat{B}li \frac{N_s}{2} \sin p\theta \cos(p\theta - \alpha) d\theta \dots \dots \dots (4.32)$$

Together with the corresponding force on the opposite element, this force produces a couple  $2Fr_1$  on the stator. An equal and opposite couple acts on the rotor and the total electromagnetic torque on the rotor is the integral of the elementary contributions over the whole airgap periphery: over  $p$  pole-pairs

$$\begin{aligned} T &= -p \int_0^{\pi/p} 2Fr_1 d\theta \\ &= -2r_1 Bli \frac{N_s}{2} \int_0^{\pi} \sin \theta \cos(\theta - \alpha) d\theta \\ &= -\frac{\pi r_1 Bli N_s}{2} \sin \alpha \text{ Nm} \dots \dots \dots (4.33) \end{aligned}$$

Maximum Positive torque is obtained when  $\alpha = -\pi/2$  that is with the rotor north d-axis 'lagging' 90 electrical degrees behind the axis of the stator ampere-conductor distribution.

This analysis has been carried out for a stationary stator winding. To produce a constant torque with the rotor rotating at a steady speed, the stator ampere-conductor distribution must be made to rotate in synchronism with the rotor. This is done exactly as in induction motors, by means of a poly phase winding supplied with poly phase balanced currents. The most common number of phases is three, but two-phase motors are sometimes built, and occasionally four, six, and nine-phase motors.

With  $p$  pole-pairs, if  $N_p = N_s/2p$  is the number of sine-distributed turns per pole, the total number of turns per phase is  $N_s$ . If the phase current flows through all these in series, then with balanced sine wave

currents and three phase windings whose axes are 120 electrical degrees apart, the rotating ampere-conductor distribution can be derived as

$$\hat{i} \cos \omega t \frac{N_s}{2} \sin P\theta + \hat{i} \cos\left(\omega t - \frac{2\pi}{3}\right) \frac{N_s}{2} \sin\left(P\theta - \frac{2\pi}{3}\right) + \hat{i} \cos\left(\omega t + \frac{2\pi}{3}\right) \frac{N_s}{2} \sin\left(P\theta + \frac{2\pi}{3}\right) = \frac{3}{2} I \sqrt{2} \frac{N_s}{2} \sin(P\theta - \omega t) \dots \dots \dots (4.34)$$

and the rotating magnet flux distribution is

$$B(\theta) = \hat{B} \cos(P\theta - \omega t - \alpha) \dots \dots \dots (4.35)$$

The torque is obtained using the same expression as for the stationary winding, with  $p\theta - \omega t$  substituted for  $p\theta$ , thus

$$T = \frac{3}{2} I \sqrt{2} \frac{\pi r_1 l \hat{B} N_s}{2} \sin \beta \dots \dots \dots (4.36)$$

Where  $\beta = -\alpha$ . The angle  $\beta$  is called the torque angle, and is positive for motoring; it is measured in electrical radians or degrees. If the phase winding is divided into 'a' parallel paths, then the equation remains valid provided that I is the total phase current and there is no change in the total number of turns per phase, i.e.  $N_s$ . (The number of turns in series per phase is then  $N_s/a$ .)

It is worth emphasizing that the flux-density  $\hat{B}$  in the torque equation is the peak airgap flux-density produced by the magnet acting alone; in other words, it is the open-circuit value and does not include any contribution due to the m.m.f. of the stator currents. Although the armature-reaction m.m.f. modifies the airgap flux-density, it does not figure in the torque expression unless it significantly affects the saturation level of the magnetic circuit. Physically the stator may be regarded as being incapable of producing torque on itself. The armature reaction flux is aligned with the stator ampere-conductor distribution and therefore has an effective 'torque angle' of zero.

In normal operation the stator frequency (in rad/sec) is made equal to the rotation frequency (in electrical rad/sec), i.e.,

$$\omega = 2\pi f \text{ electrical rad/sec}$$

and the mechanical angular velocity is

$$\omega_M = \frac{\omega}{p}$$

The stator ampere-conductor distribution rotates in synchronism with the rotor and the torque angle is kept constant, usually by means of a simple form of 'vector' control or 'field-oriented control' which requires a

shaft position sensor (i.e. encoder or resolver feedback). If the supply frequency and the rotation frequency were unequal, the motor would be running asynchronously. No average torque would be produced, but there would be a large alternating torque at the 'beat' frequency or pole-slipping frequency.

**EMF Equations**

The e.m.f. equation of the sine wave motor can be derived by considering the e.m.f. induced in the elementary group of conductors in Fig. 4.19. Noting that Fig. 4.19 is drawn for a two-pole machine ( $p = 1$ ), for a machine with  $p$  pole-pairs in series this e.m.f. is

$$de = B(\theta)l\omega_m r_1 \frac{N_s}{2} \sin p\theta d\theta \dots\dots\dots(4.37)$$

But

$$B(\theta) = \hat{B} \cos(p\theta - \omega t - \alpha) \dots\dots\dots(4.38)$$

and by integrating the contributions of all the elementary groups of conductors we get the instantaneous phase e.m.f.:

$$e = 2p \int_0^{\pi/p} de = \frac{\hat{B}l\omega r_1 N_s \pi}{2p} \sin(\omega t + \alpha) \dots\dots\dots(4.39)$$

The R.M.S. phase e.m.f. is therefore

$$E_{ph} = \frac{\pi}{2\sqrt{2}} \frac{\hat{B}l\omega r_1 N_s}{p} V_{r.m.s} \dots\dots\dots(4.40)$$

and the line-line e.m.f. is  $E\sqrt{3}$

It is worth emphasizing again that the flux-density  $\hat{B}$  is the peak airgap flux-density produced by the magnet acting alone; in other words, it is the open-circuit value and does not include any contribution due to the m.m.f. of the stator currents. The voltage drop induced by flux attributable to armature reaction is dealt with below.

The e.m.f. equation can also be derived from Faraday's law. This alternative method is included here because it is the basis of the phasor diagram and provides the means for calculating the inductive volt drop due to armature reaction. Faraday's law is more rigorous than the BLV formulation, but it is useful to show that for  $E$  both methods give the same result. By Faraday's law, the instantaneous e.m.f. induced in the stationary phase winding of Fig. 4.19 is given by

$$e = -\frac{d\psi}{dt} V \dots\dots\dots(4.41)$$

Where  $\psi$  is the instantaneous flux-linkage. To calculate the flux-linkage consider the coil formed by the elementary group of conductors within the angle  $d\theta$  at angle  $\theta$ , and assume that the return conductors of this coil are located within the angle  $d\theta$  at angle  $-\theta$ . Although Fig. 4.19 is drawn for a two-pole machine ( $p = 1$ ), the results are derived for  $p$  pole-pairs.

On open-circuit there is no current in the coil, and all the flux is due to the magnet. The flux through the elementary coil is

$$\phi = \int_{-\theta}^{\theta} B(\theta) r_l d\theta \text{ Wb} \dots \dots \dots (4.42)$$

But

$$B(\theta) = \hat{B} \cos(p\theta - \omega t - \alpha)$$

So the integral gives

$$\phi = \frac{\hat{B} D l}{p} \sin p\theta \cos(\omega t + \alpha) \text{ Wb} \dots \dots \dots (4.43)$$

Where  $D = 2r_l$  is the stator bore. The flux per pole can be extracted from this expression by setting  $\theta = \pi/p$  and  $t = 0$ . Thus

$$\phi_M = \frac{\hat{B} D l}{p} \text{ Wb} \dots \dots \dots (4.44)$$

This is a fixed flux that rotates with the rotor. The flux-linkage of the elementary coil is

$$d\psi = \phi \left[ \frac{N_s}{2} \sin p\theta d\theta \right] \text{ Vs} \dots \dots \dots (4.45)$$

The total flux-linkage of the winding is obtained by integrating the contributions of all the elementary coils: with  $p$  pole-pairs the result is

$$\psi_M = p \int_0^{\pi/p} d\psi = \hat{\psi}_M \cos(\omega t + \alpha) \text{ Vs} \dots \dots \dots (4.46)$$

Where

$$\hat{\psi}_M = \frac{\hat{B}l r_1 N_s \pi}{2p} = \frac{\pi}{4} N_s \phi_M V_s \dots \dots \dots (4.47)$$

The subscript 'M' has been added as a reminder that the flux is produced only by the magnet. By Faraday's law the instantaneous phase e.m.f. is

$$e = -\frac{d\psi_M}{dt} = \omega \hat{\psi}_M \sin(\omega t + \alpha) V \dots \dots \dots (4.48)$$

The R.M.S. phase e.m.f. is

$$E_{ph} = \frac{\omega \hat{\psi}_M}{\sqrt{2}} = \frac{\pi}{2\sqrt{2}} \frac{\hat{B}l \omega r_1 N_s}{p} V_{r.m.s} \dots \dots \dots (4.49)$$

**4.8 Torque-speed characteristics**

Ideal motors were considered in the analysis above; in practice, the construction of the stator windings, and particularly the effect of the stator's slots, has a significant effect on the motor's performance and characteristics. In addition, the location of the magnets either mounted on the surface or within the body of the rotor, has to be considered in detail.

The torque equation can also be expressed in the form;

$$T = \frac{p E_p I \sin \beta}{\omega_s} \dots \dots \dots (4.50)$$

and hence

$$\omega_m T = 3 E_p I \sin \beta \dots \dots \dots (4.51)$$

The overall torque-speed characteristics of the motor derived from this equation is shown in Figure 4.20. The peak torque can be maintained up to the base speed. Above this speed, by modifying  $\beta$ , the motor will effectively enter a field weakening mode, allowing an increase in the speed at the expense of the peak torque. The motor's efficiency is reduced in this region because the motor is being supplied with the peak current.

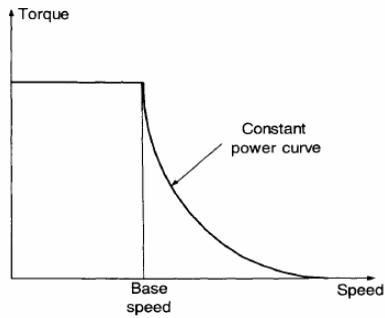


Figure 4.20 Torque Speed Characteristics of PMSM

## 4.9 PERMANENT MAGNET DC COMMUTATOR MOTORS

### 4.9.1 CONSTRUCTION

A D.C. PM Commutator motor can be compared with a D.C. separately excited motor. The only difference is in the excitation flux  $\phi_g$  in the air gap: for a PM motor  $\phi_g = const$  whilst for a separately excited motor  $\phi_g$  can be controlled. This means that the speed of a standard D.C. PM commutator motor can normally only be controlled by changing the armature input voltage or armature current. A typical D.C. PM Commutator motor is shown in Fig. 4.1(b). By adding an additional field excitation winding, the flux  $\phi_g$  as well as the speed can be changed in a certain limited range. *Alnico* PMs used to be common in motors having ratings in the range of 0.5 to 150 kW. Ceramic magnets are now most popular and economical in fractional horsepower motors and may have an economic advantage over *Alnico* up to about 7.5 kW. Rare-earth magnet materials are costly, but are the best economic choice in small motors. Magnetic circuit configurations of different types of PM D.C. commutator motors are shown in Fig 4.21. There are four fundamental armature (rotor) structures:

- ✓ Conventional slotted rotor (Fig. 4.2a).
- ✓ Slot less (surface wound) rotor (Fig. 4.2b).
- ✓ Moving-coil cylindrical rotor.
- ✓ Moving-coil disk (pancake) rotor.

The slotted- and slot less-rotor PM commutator motors have armature windings fixed to the laminated core. The armature winding, armature core and shaft create one integral part.

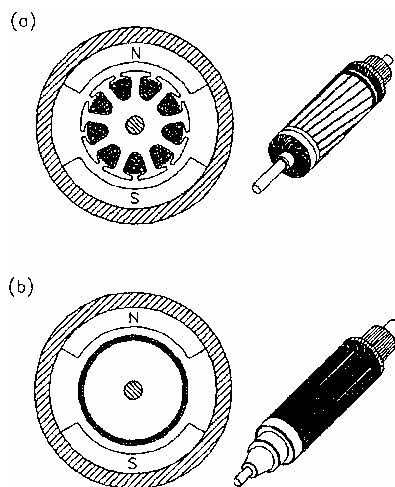


Figure 4.21: Construction of d.c. PM commutator motors with laminated- core rotors: (a) slotted rotor, (b) slot less rotor.

### **4.9.1.1 Slotted-rotor PM D.C. motors**

The core of a slotted rotor is a lamination of silicon steel sheet or carbon steel sheet. The armature winding is located in the rotor slots. The torque acts on the conductors secured in the slots and reinforced by the slot insulation and epoxy resin. Thus a slotted rotor is more durable and reliable than a slot less rotor (Fig. 4.2a). A core having many slots is usually desirable, because the greater the number of slots, the less the cogging torque and electromagnetic noise. Cores having even numbers of slots are usually used for the motors manufactured by an automated mass production process because of the ease of production. From the motor quality point of view, ferromagnetic cores with odd numbers of slots are preferred due to low cogging torque.

### **4.9.1.2. Slot less-rotor PM motors**

Extremely low cogging torque can be produced by fixing the windings on a cylindrical steel core without any slots (Fig. 4.2b). In this case the torque is exerted on the conductors uniformly distributed on the rotor surface. However, the flux decreases in comparison with the slotted rotor since the gap between the rotor core and the pole shoes is larger. Therefore, larger volume of PMs must be used to get sufficient magnetic flux.

## **4.10 TORQUE AND EMF EQUATIONS**

### **4.10.1 TERMINAL VOLTAGE**

From the Kirchhoff's voltage law, the terminal (input) voltage is

$$V = E + I_a \sum R_a + \Delta V_{br} \dots \dots \dots (4.52)$$

Where  $E$  is the voltage induced in the armature winding (back EMF),  $I_a$  is the armature current,  $\sum R_a$  is the resistance of the armature circuit and  $\Delta V_{br}$ , is the brush voltage drop. The brush voltage drop is approximately constant and for most typical D.C. motors is practically independent of the armature current.

### **4.10.2 ARMATURE WINDING EMF**

The EMF induced in the armature winding by the main flux  $\phi_g$  in the air gap is

$$E = \frac{N}{a} pn\Phi_g = c_E n\Phi_g \dots \dots \dots (4.53)$$

Where  $N$  is the number of armature conductors,  $a$  is the number of pairs of armature current parallel paths,  $p$  is the number of pole pairs,  $\phi_g$  is the air gap (useful) magnetic flux, and



$$c_E = \frac{N_p}{a} \dots\dots\dots(4.54)$$

is the *EMF constant* or *armature constant*. For a. PM excitation  $K_E = c_E \Phi_g = \text{Constant}$ , thus

$$E = K_E n \dots\dots\dots(4.55)$$

The following relationship exists between the number of armature conductors N and the number of commutator segments C:

$$N = 2CN_c \dots\dots\dots(4.56)$$

Where  $N_c$  is the number of turns per armature coil

**4.10.3 ELECTROMAGNETIC (DEVELOPED) TORQUE**

The electromagnetic torque developed by the D.C. commutator motor is

$$T_d = \frac{N}{a} \frac{p}{2\pi} \phi_g I_a = c_T \phi_g I_a \dots\dots\dots(4.57)$$

where

$$c_T = \frac{Np}{2\pi a} = \frac{c_E}{2\pi}$$

is the *torque constant*. The electromagnetic torque is proportional to the armature current. PMs produce a constant field flux  $\phi_g = \text{const}$  (neglecting the armature reaction). The developed torque is

$$T_d = k_T I_a \dots\dots\dots(4.58)$$

where

$$k_T = c_T \phi_g$$

**TWO MARKS QUESTIONS AND ANSWERS**

1. Mention the kinds of permanent magnet used in BLDC motor.
  - Alnico magnet
  - Ferrite or ceramic magnet
  - Rare earth magnet (Samarium cobalt magnet)
2. Mention the types of Permanent Magnet motors.
  - ✓ DC Commutator motor drives.
  - ✓ Brushless motor drives.
    - Square Wave Permanent magnet brushless motor drives (also called as PMBLDC).
    - Sine Wave Permanent magnet brushless motor drives (also called as PMSM).
  - ✓ Stepping motor drives.
3. Why is a BLDC motor called a dc motor?

Because in a BLDC motor the stator and the rotor fluxes maintain a constant angle, although both are rotating in space. This is similar to the dc motor, but in the dc motor, both the armature and the field flux are stationary in space.

4. Why does a BLDC motor come with an integrated hall sensor?

Because, to maintain a constant angle difference between the stator and the rotor flux, the stator current has to be switched from winding to winding depending on the rotor position. So the rotor position is sensed in all BLDC motors, by the Hall sensors.

5. What are the reasons behind the popularity of BLDC motors over dc motors for servo applications?

Higher torque to weight ratio, due to rare earth magnets which have less weight and have much higher operating flux density limits. This leads to faster dynamic response. Also, the lack of brushes and commutators reduce maintenance problems.

6. Name application areas where a BLDC motor drive is preferable over an ac drive.

Most control applications are examples, such as, CNC control, Avionic controls etc.

7. Mention the advantages of brushless configuration.

- ✓ No brushes. So no brush maintenance and no problem of RFI.
- ✓ Rotor is inside the stator. So more cross sectional area is available for the power or armature winding.
- ✓ Conduction of the heat through the frame is improved.
- ✓ Increase in electric loading is possible.
- ✓ Torque developed is high.
- ✓ Efficiency is higher than commutator motor because of the absence of brush friction.
- ✓ Motor length is reduced. So less space occupation, reduction in the length between the bearings.
- ✓ The removal of the commutator reduces the inertia.
- ✓ No field winding. So no field copper loss.
- ✓ Stability is good and easy to cool.

8. Write the disadvantages of brushless configuration.

- Shaft position sensing is needed
- Electronic controller design becomes more complex.

9. Why the flux linkage curve is linear in PMSM motor?

The flux linkage varies linearly with rotor position because the air gap flux density set up by the magnet is constant over each pole pitch of the motor.

10. Define fringing.

When the lines of flux pass from one pole to another pole through the (air gap) non magnetic medium it bulges out from its original path which results the increase in the air gap flux area. This effect is called fringing.

11. What is the effect of fringing in the emf wave form of PMBLDC motor?

In practice the fringing causes the corners of the emf wave to be rounded. This results the trapezoidal shape in that wave.

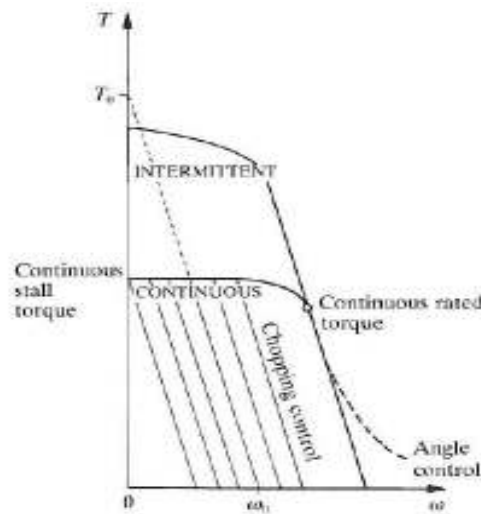
12. What is electronic commutator?

The device which is used for the commutation process in the PMBLDC motor with the help of power electronic switches is called as electronic commutator.

13. List the disadvantages of commutator motor.

- a. Formation of dust, which forms the conducting track and leads to flash over.
- b. The operation and life of the brushes depend on the atmospheric condition.
- c. Different brush grades should be used in the same motor for different atmospheric condition.

14. Draw the speed torque characteristics of PMBLDC motors



15. Write the EMF and Torque Equations of PMBLDC motors

**EMF Equation**

$$e_1 = 2N_{ph}B_g l r_1 \omega [Volts]$$

Where  $N_{ph}$  is the number of turns in series per phase. In this case  $N_{ph} = 2N_1$

**TORQUE EQUATION**

$$T_e = 4N_{ph}B_g l r_1 I [Nm]$$

16. How PMSM differs from PMBLDC

The sine wave motor differs in all three respects. It has:

- ✓ Sinusoidal or quasi-sinusoidal distribution of magnet flux in the air gap;
- ✓ Sinusoidal or quasi-sinusoidal current waveforms;
- ✓ Quasi-sinusoidal distribution of stator conductors; i.e. short-pitched and distributed or concentric stator windings.

17. Write the EMF and Torque Equations of PMSM motors

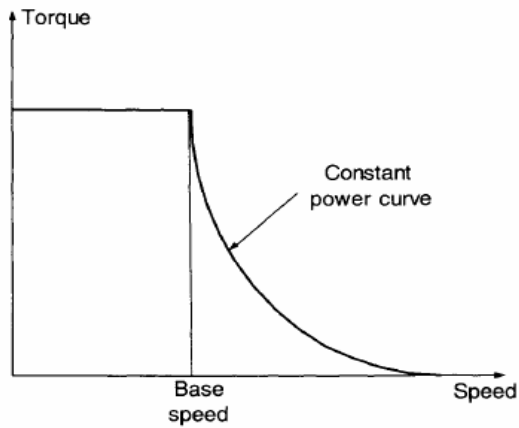
**EMF Equation**

**Torque Equation**

$$E_{ph} = \frac{\omega \hat{\psi}_M}{\sqrt{2}} = \frac{\pi}{2\sqrt{2}} \frac{\hat{B} l \omega r_1 N_s}{p} V_{r.m.s}$$

$$T = \frac{3}{2} I \sqrt{2} \frac{\pi r_1 \hat{B} N_s}{2} \sin \beta$$

18. Draw the Speed torque Characteristics of PMSM motors



19. Draw the speed torque characteristics of PMDC motors

